LATE CENOMANIAN – EARLY TURONIAN RECONSTRUCTION OF INTERMEDIATE AND DEEP-WATER CIRCULATION IN THE PROTO-INDIAN OCEAN

A Thesis

by

DAVID STEVEN TILGHMAN

Submitted to the Office of Graduate and Professional Studies of
Texas A&M University
in partial fulfillment of the requirements for the degree of

MASTER OF SCIENCE

Chair of Committee,	Deborah Thomas
Committee Members,	Thomas Olszewski
	Franco Marcantonio
Head of Department,	John R. Giardino

December 2013

Major Subject: Geology

ABSTRACT

The late Cenomanian and early Turonian (~96-90 Ma) was an interval characterized by a global warming trend and peak sea surface temperatures during the Mesozoic and Cenozoic eras. The Cenomanian/Turonian boundary (~94 Ma) also coincided with widespread burial of organic carbon (Oceanic Anoxic Event 2 - OAE2). Several factors likely promoted organic carbon burial including increased nutrient input, diminished seafloor oxygen levels, density stratification, enhanced upwelling, and sluggish deep-water circulation. A growing body of Nd isotope data is constraining the role of deep-water circulation in organic carbon burial during OAE2. An increase in deep-water $\varepsilon_{Nd}(t)$ values across the C/T in the tropical Atlantic is interpreted to reflect a change in deep-water circulation that may have led to higher sea surface nutrient levels, suggesting deep-water circulation was not sluggish. Furthermore, previously published low-resolution Nd isotope data from proto-Indian Ocean ODP Sites 763, 765, 766, and 1138 suggested a change during the mid-Cretaceous that may have coincided with the C/T.

Here we present new high-resolution data from the proto-Indian Ocean Sites to determine the evolution and timing of intermediate- and deep-water Nd isotope values. Deep-water $\varepsilon_{Nd}(t)$ values from Site 765 and 766 (3000-4000m paleowater depth) vary coherently between ~-8.5 and ~-5.5 over the interval ~98 to 91 Ma. These sites record a gradual 1.5 epsilon unit increase throughout the study interval. The evolution of intermediate-water $\varepsilon_{Nd}(t)$ values in the region were significantly different from the deep-

water values. Site 763 $\varepsilon_{Nd}(t)$ values ranged from ~-10.5 to -11.1 from 95.8 to 92.4 Ma, then increased to -7.1 by 89.8Ma. In the western portion of the basin, intermediate-water values recorded at Site 1138 decreased from -4.4 to -6.7 from ~95 to 93 Ma. Late Cretaceous sea level transgression and extreme global warmth, based on $\delta^{18}O$ data, are both contributing factors to the vertical expansion of warm surface waters displayed by the new data. This work shows that the oceanic response to Late Cretaceous warming varied in different regional ocean basins.

DEDICATION

To my family

&

The advancement and expansion of geoscience knowledge

ACKNOWLEDGEMENTS

I would like to thank my committee chair, Dr. Debbie Thomas, for her patience, constructive feedback, and willingness to explore alternative hypothesis. I would also like to thank my committee members, Dr. Franco Marcantonio, Dr. Thomas Olszewski, for their knowledge and wisdom throughout my time as an undergraduate and graduate student at Texas A&M.

Thanks also go to my friends and colleagues and the department faculty and staff for making my time at Texas A&M University a great experience. I also want to extend my gratitude to the Integrated Ocean Drilling Program, which provided the samples, and to R. Ken Williams ’45 for the Radiogenic Isotope Geosciences Laboratory.

NOMENCLATURE

C/T	Cenomanian/Turonian
DBW	Demerara Bottom Water
Fe-Mn	Ferromanganese Oxide Minerals
HH	Hydroxylamine Hydrochloride
LIP	Large Igneous Province
MBSF	Meters Below Sea Floor
Nd	Neodymium
OAE	Oceanic Anoxic Event
ODP	Ocean Drilling Program
SST	Sea Surface Temperature
TIMS	Thermal Ionization Mass Spectrometer

TABLE OF CONTENTS

Page

LIST OF FIGURES

CHAPTER I

INTRODUCTION

The Late Cretaceous was characterized by extreme warmth, with global temperatures peaking during the Turonian ~ 90 Ma (e.g., Wilson et al., 2002). The overall climate was characterized by lower than modern meridional thermal gradients (Huber et al., 1995; Hay, 2008; Hasegawa et al., 2011; Moriya, 2011). Furthermore, the oceanic vertical temperature gradient was also lower than modern (Wilson and Norris, 2001; Huber et al., 2002). A major transgression during the Late Cretaceous also coincided with the peak warmth. This sea level rise may have resulted from increased volcanic activity and thermal expansion of the mid-ocean ridge system, causing a rise in eustatic sea level (Schlanger and Jenkyns, 1976; Jenkyns, 1980; Jenkyns, 1985; Arthur et al., 1987; Arthur et al., 1990; Dale et al., 2011).

Global greenhouse warmth likely was related to high levels of atmospheric pCO_2 (Retallack, 2001; Haworth et al., 2005; Moriya, 2011). The range of atmospheric pCO_2 levels from 1000μ atm to 5500 μ atm (Retallack, 2001), may have been caused by higher than modern seafloor spreading rates, and the emplacement of several large igneous provinces (LIPs) that were actively forming throughout the Cretaceous (Pearce et al., 2009; Gertsch et al., 2010; Moriya, 2011; Monteiro et al., 2012).

The geologic record of the Jurassic and Cretaceous is punctuated by numerous episodes of widespread accumulation of organic rich sediments likely related to oceanic anoxia (Schlanger and Jenkyns, 1976; Jenkyns, 1980; Jenkyns, 1985; Arthur et al., 1987;

Arthur et al., 1990; Jenkyns, 2010; Jarvis et al., 2011). However, there are three episodes that have been identified on a large enough scale to be classified as major Oceanic Anoxic Events during the Mesozoic (Jenkyns, 2010): The Early Toarcian (T-OAE) ~180 Ma, the Early Aptian (OAE-1a) ~120 Ma, and the Cenomanian/Turonian (OAE2) ~94 Ma. The Cenomanian/Turonian (C/T) boundary (~94 million years ago) was characterized by global warming. OAE2 geographically and chronologically was the most intense of the anoxic events and resulted in the preservation and burial of vast amounts of organic carbon, in the form of hydrocarbon rich black shales (Schlanger and Jenkyns, 1976; Hue et al., 2001; Jenkyns, 2010; El-Sabbagh, 2011; Jarvis et al., 2011).

Dissolved oxygen in the water column as well as the seafloor is controlled by ocean temperatures, rates of microbial oxidation of organic matter, and seafloor ventilation. The idea that warm climates with low equator to pole thermal gradients were characterized by "sluggish" deep ocean circulation is not new (Huber et al., 1995; Hay, 2008; Moriya, 2011; Jarvis et al., 2011; Hasegawa et al., 2012). In theory, sluggish deep-water circulation as a result of a reduced temperature gradient and/or bathymetric barriers could have diminished ventilation of the seafloor, potentially enhancing the preservation of organic matter (e.g., Schlanger and Jenkyns, 1976; Demaison and Moore, 1980; Bralower and Thierstein, 1984; Tyson, 2005; Foster et al., 2008; Peceat 2008; Jenkyns, 2010; Jarvis et al. 2011).

However, some investigations suggest that there was little to no reduction in the intensity of thermohaline or wind-driven ocean circulation during the Cretaceous (Totman Parish and Curtis, 1982; Manabe and Bryan, 1985). For example, Manabe and

Bryan (1985) reported that simulations incorporating a reduced pole to equator temperature gradient still produced vigorous ocean circulation. This implies that bottom water formation and ocean circulation during the Cretaceous were sufficient to ventilate the deep ocean and to upwell abundant nutrients to allow for blooms in production (Kuypers et al., 2004). This presents an interesting contradiction - upwelling could have contributed ultimately to the supply of large quantities of organic carbon to the sea floor (Arthur et al., 1987; Foster et al., 2008; Hay, 2008; Alexandre et al., 2010; Jenkyns, 2010; Monteiro et al., 2012), however deep-sea ventilation would have inhibited the accumulation of that organic matter.

The formation of oceanic gateways and connections that controlled open ocean circulation may have had a significant impact on the ocean dynamics across the C/T (Poulsen, 2001). The existence of restricted basins could have developed through bathymetric barriers inhibiting ocean circulation and hence reducing dissolved oxygen delivery to the deep ocean basins during the C/T (Tissot et al., 1980; Totman Parrish and Curtis, 1982; Poulsen, 2001). Several recent studies have investigated the potential role of ocean circulation in deep-sea ventilation across the C/T. However, the majority of these studies have focused on the tropical Atlantic (MacLeod et al., 2008; Alexandre et al., 2010; Macleod et al., 2011; Martin et al., 2012). Not all oceans during the Late Cretaceous were restricted by paleobathymetric barriers (Hay et al., 1999; Heine et al., 2004). The restricted ocean model for the main cause for anoxia in this case cannot be applied to every basin either. The environmental factors that were dominant could have

varied depending on location, meaning that each ocean basin would have had a unique response to Late Cretaceous warming and OAE2.

OAEs likely required some combination of enhanced surface water production and diminished seafloor oxygenation (enhanced preservation). The name "anoxic event" implies conditions more efficient at preserving organic carbon at the seafloor than "normal" conditions (e.g., diminished seafloor oxygenation or an expanded oxygen minimum zone) (Schlanger and Jenkyns, 1976; Jenkyns, 1980; Jenkyns, 1985; Arthur et al., 1987; Jarvis et al., 1988; Arthur et al., 1990; Jenkyns, 2010; Jarvis et al., 2011). A potential modern analog of anoxic conditions is the Black Sea. Interestingly, the Black Sea has an anoxic water column, yet relatively low rates of organic carbon accumulation (Pederson and Calvert, 1990; Tyson, 2005). Thus, an explanation for OAEs likely requires some component of increased primary production along with enhanced preservation (Schlanger and Jenkyns, 1976; Jenkyns, 1980; Jenkyns, 1985; Tyson, 2005; Jenkyns, 2010; Westermann et al., 2010; Jarvis et al., 2011).

Enhanced primary production requires higher rates of nutrient delivery to the surface oceans. Increased upwelling and continental runoff, as well as the input of metals through LIP eruption are all mechanisms that may have contributed to Late Cretaceous OAEs. Furthermore, the increase in sea level would have flooded low-lying continental shelf regions, resulting in productive shallow coastal margins (Jenkyns, 1985; Dale et al., 2011).

Alternatively, recent work suggests that enhanced primary productivity alone cannot explain the global distribution of black shales during the major OAEs (Tyson,

2005; Jarvis et al., 2011). The hypothesis that ocean productivity was the driving factor in black shale deposition works only in localized zones (Wilson and Norris, 2001; Tyson, 2005). Studies have been presented supporting upwelling induced productivity (Pederson and Calvert, 1990; Tyson, 1996, Berrocoso et al., 2010, Monteiro et al., 2012) as a potential cause for anoxia development.

The fundamental question remains - what processes, global and regional, combined to promote the accumulation of anomalously high amounts of organic carbon at the seafloor during the OAEs?

Here, we propose to explore the role of deep-water circulation in organic matter preservation during a global warming trend by reconstructing the intermediate- and deep-water mass compositions in the proto-Indian Ocean. These new data will allow us to test the hypothesis that deep-ocean circulation patterns varied among the different ocean basins during the Cenomanian-Turonian interval.

To address this hypothesis and advance our general understanding of deep-ocean circulation during the Late Cretaceous, we analyzed the Nd isotopic composition of leached oxide minerals from ODP Sites 763, 765, 766, and 1138, located in the Proto-Indian Ocean off the western margin of Australia (Figure 1).

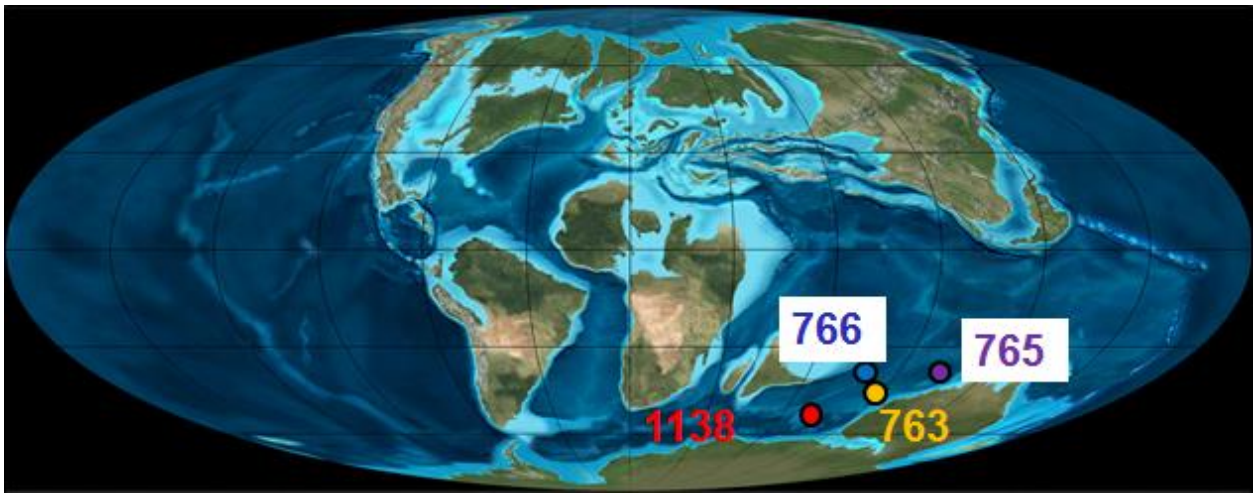

Figure 1: 90 Ma paleogeographic reconstruction (*Ron Blakey,* http://www2.nau.edu/rcb7/90moll.jpg*)* indicating the ancient locations of Sites 763, 765, 766, and 1138.

CHAPTER II

METHODS

Nd isotopes are a useful tracer for the reconstruction of deep-ocean water mass compositions (e.g., Piepgras et al., 1979; von Blanckenburg, 1999; Goldstein and Hemming, 2003). Nd has a residence time of ~1000 years (Tachikawa et al., 1999), shorter than the mixing of the ocean (~1500 years) (Broecker et al., 1960), and this promotes the development of interbasinal differences in the $^{143}Nd/^{144}Nd$ ratio (expressed as ε_{Nd} which has been normalized to the bulk earth, DePaolo and Wasserburg, 1976).

$$\varepsilon_{Nd} = \left[\frac{\left(\frac{^{143}Nd}{^{144}Nd}\,\text{SAMPLE}\right) - \left(\frac{^{143}Nd}{^{144}Nd}\,\text{CHUR}\right)}{\frac{^{143}Nd}{^{144}Nd}\,\text{CHUR}} \right] 10{,}000\,,$$

Equation 1: The equation used to normalize the Nd ratios for analysis. The present day Chondritic Uniform Reservoir (CHUR) value is 0.512658

The primary source of dissolved Nd to the oceans is fluvial inputs of weathered subaerially exposed terranes (Goldstein et al., 1988). Hydrothermal Nd contributions are negligible due to scavenging (Halliday et al., 1992). Thus, intermediate- and deep-water masses acquire the Nd signature of the surface waters in the region in which they form, which, in turn, are derived from the rivers draining into a particular region (Goldstein et al., 1988). The Nd signature is largely retained as the water mass circulates through the ocean basins (e.g., Piepgras et al., 1979; von Blanckenburg, 1999).

Temporal changes in weathering inputs to the water mass source region can alter the water mass Nd signature in a given location (Goldstein et al., 1988). Changes in the water mass Nd signature can also result from water mass mixing (von Blanckenburg, 1999), boundary exchange (Lacan and Jeandel, 2005; Zhang et al., 2008), and/or detrital overprinting.

Ferromanganese (Fe-Mn) oxide minerals precipitate on sediments at the seafloor and incorporate the Nd signature at the sediment water interface at the time of deposition (Palmer and Elderfield, 1986; Basak et al., 2011). Measuring the Nd preserved in Fe-Mn oxide minerals within a given sediment sequence permits reconstruction of the water mass composition through time. The target stratigraphic interval was from 100Ma-90Ma based on the age model generated by Murphy and Thomas (2012). Site 763 was at a paleowater depth of around 1000m, with Sites 766 and 765 estimated at 3000m and 4000m, respectively (Figure 1). Site 1138 was located on the western edge of the thermally subsiding Kerguelen Plateau with a final paleowater depth in the intermediate water range of 500m (85 Ma) (Figure 1). At Site 763 we analyzed 19 samples over an interval from 355.1 meters below sea floor (mbsf) (88.5 Ma) to 442.4 mbsf (100.8 Ma). At Site 765 we analyzed 12 samples from 582.6 mbsf (89.7 Ma) to 594.2 mbsf (101.2 Ma), and at Site 766 we analyzed 12 samples from 130.1 mbsf (91.0 Ma) to 140.2 mbsf (98.9 Ma). We analyzed 17 samples from Site 1138 from 632.2 mbsf (85.9 Ma) to 689.8 mbsf (94.1 Ma).

Ferromanganese oxide minerals (Fe-Mn) were extracted from sediment samples by leaching 0.5g of homogenized bulk sample powder in dilute acetic acid buffered with

sodium acetate to a pH of ~5. The decarbonated samples were rinsed three times in ultra pure water and then leached in a buffered and dilute Hydroxylamine Hydrochloride (HH) solution following the methods of Basak et al., (2011). The leachate containing the dissolved oxide fraction was dried and then redissolved in preparation for two-stage column chemistry to isolate Nd from the rest of the cations. First, the bulk suite of rare earth elements was isolated in RE Spec cation exchange column chemistry, and then Nd was isolated through Ln Spec chromatographic chemistry.

All data analysis was performed in the R. Ken Williams '45 Radiogenic Isotope Geosciences Laboratory at Texas A&M University using a Triton thermal ionization mass spectrometer (TIMS). All data is presented as $\varepsilon_{Nd}(t)$, which has been normalized to the bulk earth and corrected for age to account for postburial decay of ^{147}Sm. External precision has been based on replicates of the JNd_i standard (n=40 during the course of this study), which produced a value of 0.512104 (15ppm 2σ).

CHAPTER III

RESULTS

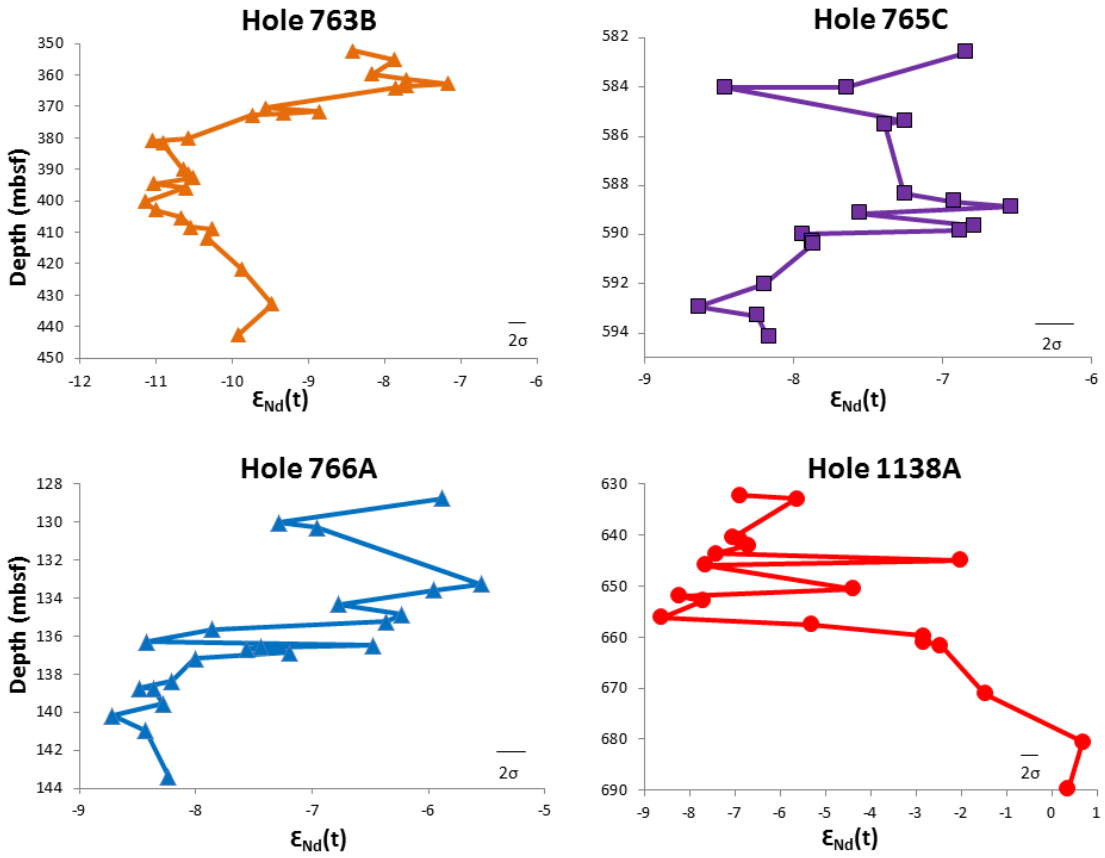

Figuer 2: $\varepsilon_{Nd}(t)$ values presented for Sites 763B, 765C, 766A, and 1138A in meters below sea floor (mbsf) from the time span equivalent of 100Ma to 90Ma.

The isotopic composition recorded at Site 763 (paleo-water depth 1000m) decreases from ~-9.9 at 442.3 mbsf to ~-11.1 at 400.1 mbsf (Figure 2). Site 763 $\varepsilon_{Nd}(t)$ values remain relatively constant from 400.1 mbsf to 380.1 mbsf before increasing to ~-7.1 at 362.7 mbsf. From 362.7 mbsf to 352.3 mbsf the $\varepsilon_{Nd}(t)$ values remain between ~-8 to -7.

Site 765 (paleo-water depth 4000m) exhibits a 2 epsilon unit increase from ~-8.6 to ~-6.5 from 592.9 mbsf to 588.8 mbsf (Figure 2). Values range between ~-6.5 and to ~-7.3 From 588.8 to 585.3 mbsf, then decrease to ~-8.4 at 584.0 mbsf. Above 584.0 mbsf, the water mass composition increases back to ~-6.8 epsilon units at the top of the study interval (~582.6 mbsf).

The isotopic composition recorded at Site 766 (paleo-water depth 3000m) ranged between ~-8.0 and ~-8.7 epsilon units from 143.3 to 137.2 mbsf. Site 766 $\varepsilon_{Nd}(t)$ values vary between ~-8.5 and ~-6.5 between 136.4 and 135.6 mbsf, then increase to ~-5.5 by ~133.3 mbsf. Continuing upsection, the $\varepsilon_{Nd}(t)$ value recorded at Site 766 decreases to ~-7.3 at 130.1 mbsf then increases to ~-5.9 at the top of the study interval (128.8 mbsf) (Figure 2).

Site 1138 on the Kerguelen Plateau recorded the water mass composition as the seafloor transitioned from ~ 0m (95 Ma) to ~500 m (85 Ma) paleo-water depth (Coffin, 1992). The isotopic composition decreased from ~0.7 to ~-8.6 from 689.8 to 656.2 mbsf. From 656.2 to the top of the study interval (~632.2 mbsf) the isotopic composition gradually increased to ~-6.9, punctuated by two abrupt increases at 650.6 and 644.9 mbsf (Figure 2).

CHAPTER IV

DISCUSSION

4.1 Evolution of regional water mass composition during the C/T interval

Sites 763, 765, and 766 form a depth transect off the western margin of Australia, with Site 1138 situated to the east on the Kerguelen Plateau. Site 763, located in intermediate water depths (~1000m), records a long term decrease in $\varepsilon_{Nd}(t)$ values from ~-9.9 at 100.8 Ma to ~-11.1 at 95.1 Ma (Figure 3) (Gradstein, 1992). Site 763 $\varepsilon_{Nd}(t)$ values remained relatively constant from 95.1 Ma to 92.5 Ma and then increased to ~-7.2 by ~89.7 Ma and remained ~-8 through the rest of the study interval. In contrast to the shallower Site 763, deep-water Site 765 (~4000m) recorded a slight overall increase in water mass composition from ~-8.2 to ~-6.9 through the study interval, with a few shorter term ~1 epsilon unit shifts between ~94.7 and 93.8 Ma. Site 766 (~3000m) recorded a ~2 epsilon unit increase over the same interval (from 99.4 to 87.1 Ma) with higher frequency oscillations evident between ~95.0 and 91.0 Ma. The data indicate that Sites 765 and 766 recorded similar values and trends throughout most of the study interval, confirming the hypothesis that both deep sites were influenced by the same water mass (Murphy and Thomas, 2012). The high-resolution differences recorded by the two sites likely resulted from uncertainties in the age models and differences in sampling resolution.

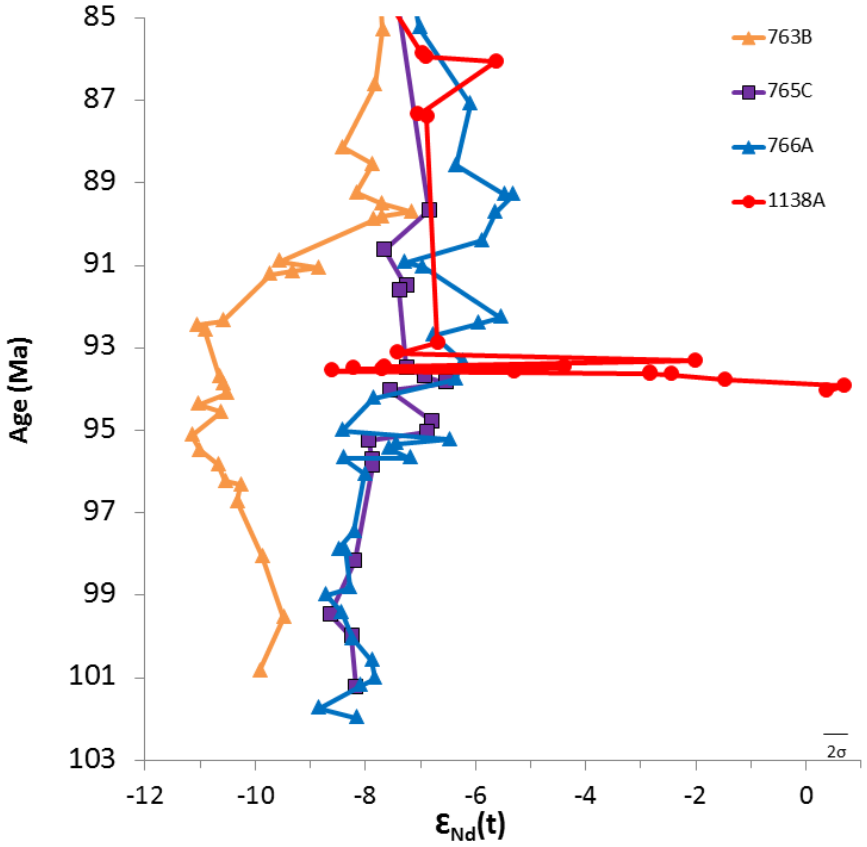

Figure 3: $\varepsilon_{Nd}(t)$ data from Site 763, 765, 766, and 1138 showing sample times produced from the age model established by Murphy and Thomas (2012).

While the regional deep Sites 765 and 766 recorded the same water mass, the trends and values were distinct from shallower Site 763 for much of the study interval. Although it is difficult to constrain the water mass composition at Site 763 prior to ~100 Ma, the available data suggest that the water mass compositions recorded at Sites 763 and 765/766 began to diverge at the base of the study interval at ~98 Ma. The shallow and deep water compositions may well have been distinct prior to this, as there is a ~1 to 2 epsilon unit offset between the intermediate- and deep-water regions at the base of the study interval. Regardless of the timing of the onset of the divergence, the regional

intermediate water composition decreased to ~-11 with minimum values recorded between ~95.1 and 92.5 Ma. The intermediate water values then increased and converged with the deep-water value recorded at Site 765. This overall regional pattern suggests different intermediate and deep-water mass compositions in the Proto-Indian Ocean during much of the early Late Cretaceous with the greatest difference evident between ~95.8 and 92.4 Ma.

Site 1138, located on the Central Kerguelen Plateau to the west of Sites 763, 765, and 766, transitioned from shallow to intermediate water depths as the seafloor underwent thermal subsidence over the interval ~94.1 Ma to 85.9 Ma (689.8 mbsf – 632.2 mbsf). The base of the 1138 record indicates rapid and large variations in the seawater isotopic composition, with $\varepsilon_{Nd}(t)$ values ranging from ~+0.7 to ~-8.6. The highly sporadic composition at Site 1138 from ~94.1 to ~92.9 Ma likely resulted from subaerial exposure of nearby portions of the Central Kerguelen Plateau resulting in the strong influence of local radiogenic weathering inputs (Meyers et al., 2009; Murphy and Thomas, 2012). Lava flows and wood fragments found within the basal sediments at Site 1138 indicate an initial period of subaerial exposure (Frey et al., 2002; Meyers et al., 2009). While Site 1138 recorded marine sedimentation by ~92.9 Ma (640.5 mbsf), other portions of the Central Kerguelen Plateau were still subaerially exposed. By ~92.8 Ma the 1138 signature recorded $\varepsilon_{Nd}(t)$ values of ~-6.7, similar to the deep-water mass signature recorded at Sites 765 and 766.

4.2 Intermediate water mass development and possible mechanisms

Several potential mechanisms could explain the distinct intermediate and deep-water compositions evident in the western portion of the proto-Indian Ocean throughout the Late Cretaceous. One aspect of the records is particularly intriguing – the divergence between Site 763 and Sites 765/766 that peaked between ~95.1 and 92.5 Ma, followed by the increase in the isotopic composition of the water mass at Site 763 toward deeper water values. This maximum difference between the shallower and deeper sites potentially reflects the degree of stratification in the region and coincides approximately with the warming trend that peaked at the C/T interval. Comparison of the seawater Nd isotope records with eustatic sea level (Kominz et al., 2008) suggests that the increase and subsequent decrease in regional water mass stratification correlated with the major sea level trends recorded during the Late Cretaceous (Figure 4).

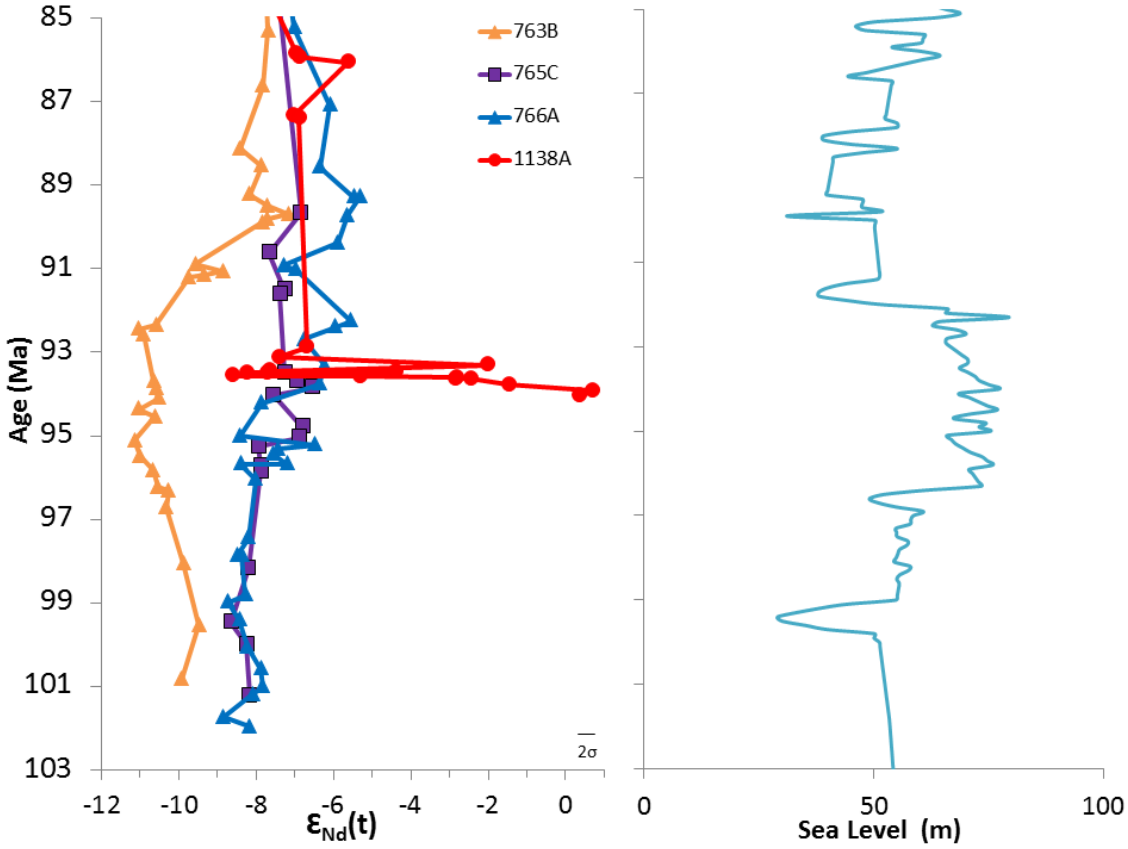

Figure 4: Nd date from Sites 763, 765, 766, and 1138 corresponding to age, based on the model produced by Murphy and Thomas 2012. Sea level (Kominz et al., 2008) (Graphed sea level data is the middle estimate with inferred lowstands) for the study interval has also been graphed to show how the sea level high stand during the Cretaceous is related to the isotopic shift seen at Site 763.

While it is not possible to determine if Sites 763, 765 and 766 all recorded the same water mass prior to the apparent increase in stratification, the correlation of the divergence of Site 763 from 765/766 with increasing sea level through the Cenomanian suggests that water mass compositions may have responded to eustatic sea level. One potential source of the isotopic decrease recorded at Site 763 was a greater influence of dissolved Nd sourced from the western margin of Australia (<~-12) (Murphy and

Thomas, 2012). Sea level rise would have flooded low lying continental regions and transported Australian continental material basinward. In fact, black shales dominated by terrestrial type III organic matter occur within the OAE2 interval at Site 763 suggesting enhanced terrigenous sediment accumulation rates (Meyers and Snowden, 1992; Meyers et al. 2009). As a consequence, enhanced terrigenous sedimentation would have increased particle scavenging and transport of unradiogenic Nd to the seafloor at intermediate water depths. If transgression caused the increase in regional continental Nd overprinting, then this effect should have diminished during the subsequent sea level fall which is the observed trend in the data.

One complication with this potential mechanism is that deep-water Site 766 was located relatively close to Site 763. If particle scavenging alone had caused the overall shift in the water mass isotope composition at Site 763 we would expect to see a similar, albeit muted, trend at Site 766. However, Site 766 recorded an overall increase in the water mass composition throughout this interval, a trend opposite that recorded at Site 763. The observation that the intermediate and deep waters in the region recorded opposite trends throughout the interval of sea level change suggests the existence of intermediate- and deep-water masses sourced from different locations.

The relatively low isotopic composition recorded at Site 763 constrains the potential source region(s) of the intermediate waters. The overall decrease to ~-11 rules out the eastern proto-Indian Ocean as source region due to the highly radiogenic weathering inputs recorded at Site 1138. We also eliminate the Pacific as a source of intermediate waters due to the relatively high isotopic composition of central Pacific

intermediate and deep waters (Thomas, 2004; Hague et al., 2012). Thus, existing Nd isotope data based on fish debris and detrital grains suggests a Southern Ocean source region for the formation of the intermediate water mass recorded at Site 763 (Murphy and Thomas, 2012; Murphy and Thomas, submitted). The Atlantic sector of the Southern Ocean was characterized by relatively low (~-11) detrital values during the Campanian and later (Robinson and Vance, 2012; Murphy and Thomas, submitted), and it is likely that such weathering inputs were similarly low during the earlier portions of the Cretaceous. However, the Atlantic sector is an unlikely source for the intermediate waters reaching Site 763 due to the path through which those waters would have advected. The Kerguelen weathering inputs that strongly impacted intermediate-water values recorded at Site 1138 would have overprinted an Atlantic-sector water mass before it reached Site 763.

The remaining potential formation region for a transient intermediate water mass, based on isotopic composition, was the Indian sector of the Southern Ocean. However, this source region would have been geographically close to the hypothesized region of deep convection that created the separate water mass bathing Sites 765 and 766. One connection we consider is that sea level rise could have altered the regional hydrography, promoting the production of separate intermediate- and deep-water masses in the Proto-Indian Ocean during the Cenomanian and early Turonian. Sea level rise may have created sufficient shelf space to enable production of shelf waters off western Australia, potentially analogous to the Demerara water mass in the Cretaceous Atlantic (MacLeod et al., 2008), or modern North Pacific Intermediate Water (Talley, 1993;

Yasuda, 1997). The challenge with applying either of these analogs to the western Australia margin is that both require some component of sea surface density increase, while sea level rise and global warming likely decreased the sea surface density field in the proto-Indian Ocean during the Cenomanian. For example, modern North Pacific Intermediate Water forms in the Okhotsk Sea, a high-latitude (50°N-60°N) restricted basin (Martin, 1998). The dense shelf waters that form in this region result from seasonal sea ice formation producing high salinity, cold waters that locally convect (Martin, 1998). It is unlikely that seasonal sea ice formation influenced intermediate-water production during the peak of Cenomanian warmth. Alternatively, shelf-water production in regions such as Demerara Rise likely required high rates of evaporation. Several studies suggest that the North Atlantic region during the C/T boundary was a potential location of mid-latitude intermediate shelf water formation (Brass et al., 1982; Haupt and Seidov, 2001; Poulsen et al., 2001; Voigt et al., 2004; Friedrich et al., 2008; MacLeod et al., 2008; Martin et al., 2012). The Northeastern European shelf was flooded during the Late Cretaceous and may have had the highest surface water density distribution within the tropical, subtropical, and midlatitude Atlantic basins (Voigt et al., 2004). This would have potentially allowed for a regional northeast shelf source of intermediate or deep-water formation in the restricted Atlantic basin (Voigt et al., 2004; Friedrich et al., 2008).

Site 763 was located in a higher, more temperate latitude setting that likely was not characterized by sufficiently high rates of evaporation to produce relatively dense shelf waters. Published bulk carbonate $\delta^{18}O$ data (Figure 5) (Clarke and Jenkyns, 1999)

help to constrain the history of regional sea surface hydrography. The $\delta^{18}O$ values indicate two general minima, with a ~.5 permil decrease from ~101.1 to 97.1 Ma, followed by a ~.5 permil increase and then another ~.5 permil decrease from ~96.4 to 94.9 Ma. The $\delta^{18}O$ data contain a sampling gap, but above the gap the record indicates a ~1 permil increase to the top of the interval of interest at ~87 Ma. In general, the Site 763 $\delta^{18}O$ data indicate relatively warm and/or low salinity waters through the C/T interval. Furthermore, the Nd isotope shift to lower values that reflects a change in the water mass composition corresponds to the second decrease in $\delta^{18}O$ values (Figure 5). Thus, the change in water mass stratification within the region likely was not related to an increase in sea surface density of shelf waters and the formation of a discrete intermediate water mass. It is interesting to note that the first $\delta^{18}O$ decrease from ~101.1 to 97.1 Ma did not correspond with a decrease in the Nd isotope values at the seafloor. This suggests that the combined influence of sea surface hydrography and sea level rise, rather than simply temperature (or salinity) alone, was key in producing the observed water mass changes.

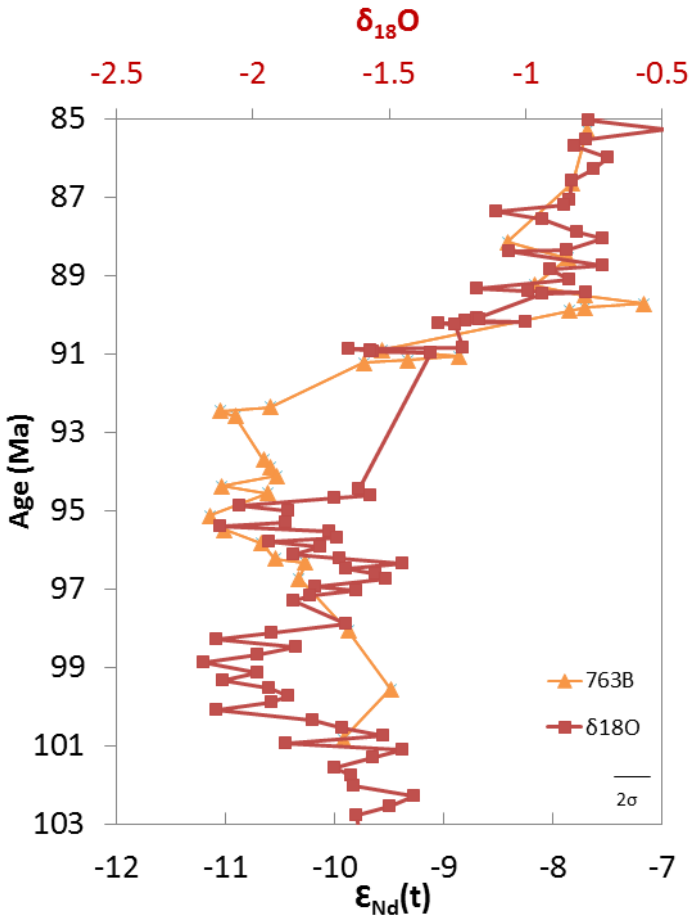

Figure 5: $\delta^{18}O$ data from Clarke and Jenkyns plotted againt Nd data from ODP site 763 to estimate sea surface temperatures in relation to the isotopic shift.

The scenario most consistent with the available data is that Site 763 recorded a deepening or thickening of a warm, low density layer coincident with peak warming and transgression (Figures 6 & 7). Thus, vertical stratification in the proto-Indian Ocean varied in concert with the combined effect of global warming and sea level rise. The extent of the warm water would have reached a minimum paleodepth of ~1000m as recorded by the $\varepsilon_{Nd}(t)$ shift seen at Site 763 and the absence of significant signature shift at 765/766.

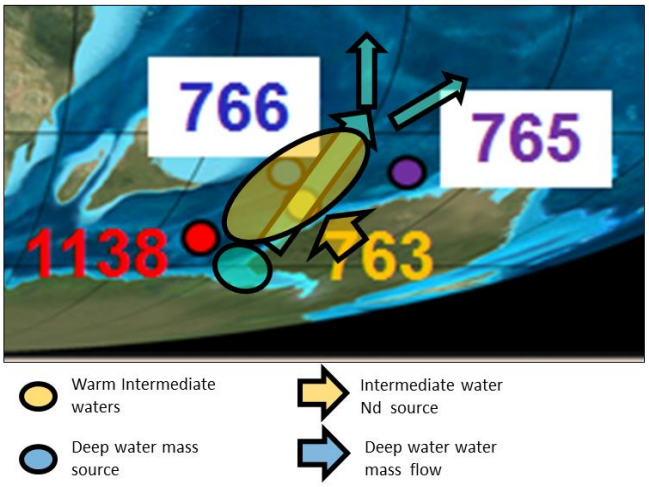

Figure 6: Paleogeographic map with water mass source regions and estimated flow direction (modified from Ron Blakey).

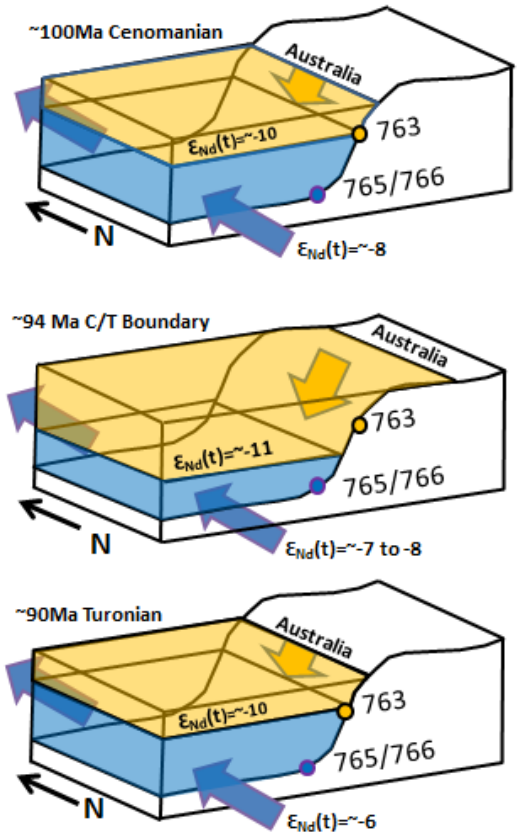

Figure 7: Schematic diagram showing the increase in depth of the warm low density layer above deep water that formed further south near the coast of Antarctica.

Site 1138 should have been positioned within the depth range of the waters that bathed Site 763, particularly if these waters reflected a thick pool of warm, low-density waters. It is likely that the transient stratification recorded at Site 763 also occurred at Site 1138, however, the isotopic composition recorded at Site 1138 was dominated by radiogenic dissolved weathering inputs from exposed portions of the Central Kerguelen Plateau.

The new data presented here extend the record of intermediate-water mass composition (recorded at Site 763) back to ~100Ma. These data suggest that the water mass bathing Site 763 was similar to that bathing deeper Sites 765/766 prior to and after the regional stratification that corresponded to the C/T warming interval (Figure 4). If the divergence between Sites 763 and 765/766 resulted from stratification, as described above, relative constancy of deep-water values suggests that the source of deep convection remained the same throughout the interval. Murphy and Thomas (2012) proposed that convection in the southern portion of the Proto-Indian Ocean between the Kerguelen Plateau and Australia produced the water mass signature recorded at Sites 765/766. The data presented here support this as the region of deep-water convection since at least ~105 Ma.

4.3 Ocean circulation during the late Cenomanian- early Turonian

Nd isotope data from Demerara Rise in the tropical North Atlantic shows a large $\varepsilon_{Nd}(t)$ increase across the C/T that has been interpreted to reflect a change in deep-water mass circulation (Figure 8) (MacLeod et al., 2008; Martin et al., 2012). The $\varepsilon_{Nd}(t)$ shift

coincides with the C/T carbon isotope excursion and the presence of finely laminated black shales (MacLeod et al., 2008; Martin et al., 2012). Data from Cape Verde, Goban Spur, Bermuda Rise, and Blake Nose within the Atlantic basin suggest that the transient Nd isotope increase recorded at Demerara Rise reflects an increase in deep-water ventilation from either the Tethys or North Atlantic. These data suggest that North and tropical Atlantic deep-water circulation was not sluggish across the C/T interval (MacLeod et al., 2008; Martin et al., 2012). In fact, the increased deep-water ventilation may have led to enhanced basinal overturning and increasing sea surface nutrient levels (Berrocoso et al., 2010; Trabucho et al., 2010; Martin et al., 2012). Thus, data from the tropical and North Atlantic basins indicate a highly dynamic oceanographic response in the Atlantic, in which enhanced overturning stimulated surface water productivity through more rapid nutrient recycling.

The detailed reconstruction of water mass structure in the proto-Indian Ocean suggests a period of transient stratification associated with peak warmth and transgression. An increase in vertical stratification would have diminished seafloor ventilation in the region of Site 763. Diminished seafloor ventilation combined with increased organic matter delivery to the region could have contributed to enhanced preservation of organic matter at the seafloor. Site 763 recorded an increase in sedimentary organic matter (ranging from 7-15% total organic carbon over the interval 385.0 to 385.7 mbsf as observed in Hole 763C) and pyrite during OAE2 (Haq et al., 1990; Bralower and Siesser, 1992; Haq et al., 1992). Thus, water mass stratification

during the late Cenomanian may have contributed to the development of OAE 2 in the region.

Late Cretaceous warming was a global event affecting every major ocean basin; however, the oceanographic conditions that resulted varied regionally. The new proto-Indian Ocean data indicates a substantially different oceanographic change during the C/T than that exhibited in the Atlantic. The observation that different oceanographic changes characterized different regions suggests that ocean circulation changes were not a global mechanism for OAE development and instead represent a response to the global processes (e.g., climate change). However, in both the Atlantic and proto-Indian oceans, the ocean circulation responses played a role in promoting organic carbon accumulation.

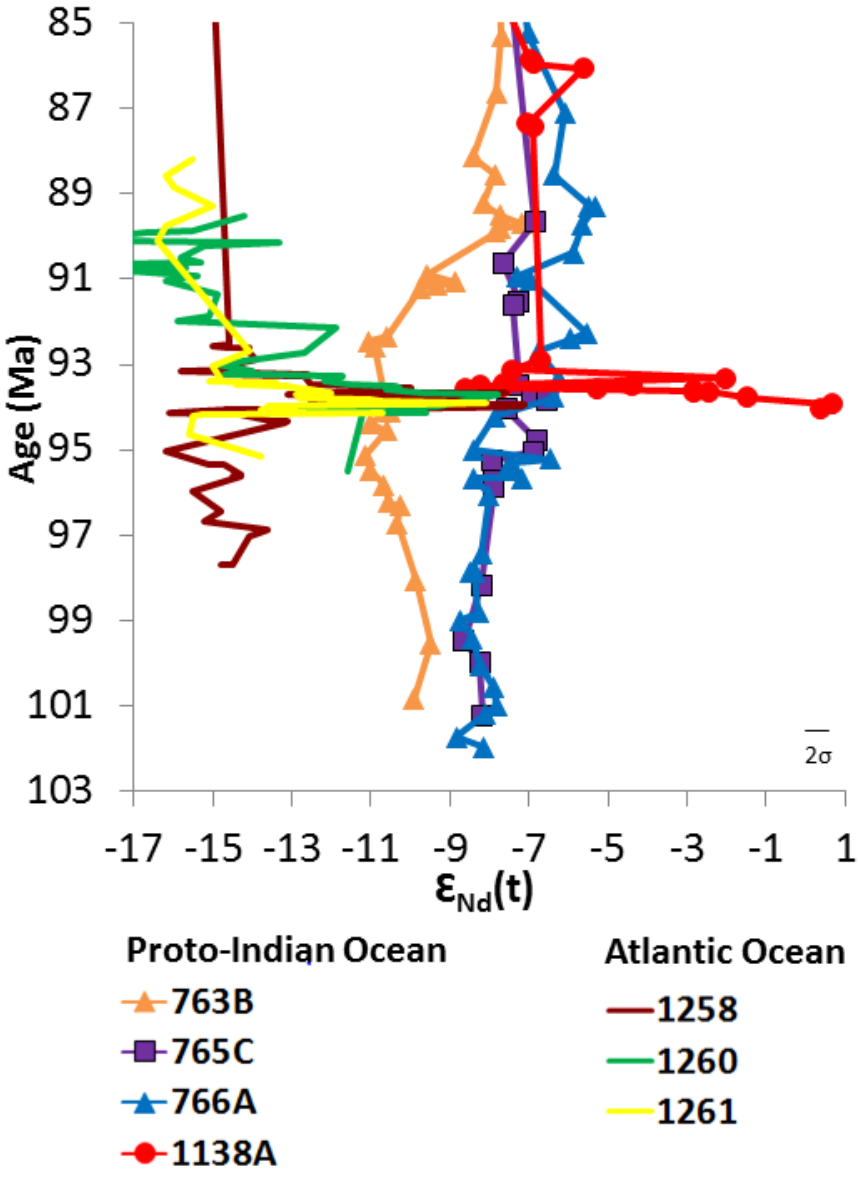

Figure 8: Comparison between the proto-Indian Ocean (Martin et al., 2012) and the Atlantic Nd isotopic composition of intermediate and deep-water during the Late Cretaceous.

CHAPTER V

CONCLUSIONS

New data from the proto-Indian Ocean records stratification of the water column from ~98.1 Ma to ~90.9 Ma coinciding with peak warmth and sea level rise during the Late Cretaceous. The Nd isotope decrease recorded at Site 763 combined with the slight increase in the isotopic composition of the deep-waters recorded at Sites 765/766 is consistent with a transient deepening of the low-density, warm surface water layer. Late Cretaceous sea level transgression and a peak in global warmth, based on $\delta^{18}O$ data, are both contributing factors in the vertical expansion of warm surface waters.

The new data provides valuable insight into the late Cenomanian – early Turonian oceanic response to global warming. This work shows that the controlling factors on black shale deposition were potentially localized to different basins. The Atlantic circulation during the C/T boundary interval shows a dynamic water column, while the proto-Indian was characterized by a more sluggish water column. Thus, the major factors contributing to ocean anoxia may have differed regionally between increased ocean productivity and decreased circulation based on the varying oceanic response.

REFERENCES

Alexandre, J. T., Tuenter, E., Henstra, G. A., van der Zwan, K. J., van de Wal, R. S., Dijkstra, H. A., and de Boer, P. L., 2010, The mid-Cretaceous North Atlantic nutrient trap: Black shales and OAEs: Paleoceanography, v. 25, no. 4.

Arthur, M. A., Jenkyns, H. C., Brumsack, H.-J., and Schlanger, S. O., 1990, Stratigraphy, geochemistry, and paleoceanography of organic carbon-rich Cretaceous sequences: Cretaceous Resources, Events and Rhythms: Background and Plans for Research, v. 304, p. 75.

Arthur, M. A., Schlanger, S. O., and Jenkyns, H. C., 1987, The Cenomanian-Turonian Oceanic Anoxic Event, II. Palaeoceanographic controls on organic-matter production and preservation: Geological Society, London, Special Publications, v. 26, no. 1, p. 401-420.

Basak, C., Martin, E. E., and Kamenov, G. D., 2011, Seawater Pb isotopes extracted from Cenozoic marine sediments: Chemical Geology, v. 286, no. 3, p. 94-108.

Berrocoso, A. J., MacLeod, K. G., Martin, E. E., Bourbon, E., Londono, C. I., and Basak, C., 2010, Nutrient trap for Late Cretaceous organic-rich black shales in the tropical North Atlantic: Geology, v. 38, no. 12, p. 1111-1114.

Bralower, T. J., and Siesser, W. G., 1992, 32. Cretaceous Calcareous Nannofossil Biostratigraphy of Sites 761, 762, and 763, Exmouth and Wombat Plateas, Northwest Australia: Proceedings of the Ocean Drilling Program, Scientific Results, v. 122, p. 614-618.

Bralower, T. J., and Thierstein, H. R., 1984, Low productivity and slow deep-water circulation in mid-Cretaceous oceans: Geology, v. 12, no. 10, p. 614.

Brass, G., Southam, J., and Peterson, W., 1982, Warm saline bottom water in the ancient ocean. Nature, v. 296, p. 620-623.

Broecker, W. S., Gerard, R., Ewing, M., and Heezen, B. C., 1960, Natural radiocarbon in the Atlantic Ocean: Journal of Geophysical Research, v. 65, no. 9, p. 2903-2931.

Clarke, L. J., and Jenkyns, H. C., 1999, New oxygen isotope evidence for long-term Cretaceous climatic change in the Southern Hemisphere: Geology, v. 27, no. 8, p. 699.

Dale, A. W., Meyers, S. R., Aguilera, D. R., Arndt, S., and Wallmann, K., 2012, Controls on organic carbon and molybdenum accumulation in Cretaceous marine sediments from the Cenomanian–Turonian interval including Oceanic Anoxic Event 2: Chemical Geology, v. 324-325, p. 28-45.

Demaison, G., and Moore, G., 1980, Anoxic environments and oil source bed genesis: Organic Geochemistry, v. 2, no. 1, p. 9-31.

DePaolo, D., and Wasserburg, G., 1976, Nd isotopic variations and petrogenetic models: Geophysical Research Letters, v. 3, no. 5, p. 249-252.

Diester-Haass, L., and Zahn, R., 1996, Eocene-Oligocene transition in the Southern Ocean: History of water mass circulation and biological productivity: Geology, v. 24, no. 2, p. 163.

El-Sabbagh, A., Tantawy, A. A., Keller, G., Khozyem, H., Spangenberg, J., Adatte, T., and Gertsch, B., 2011, Stratigraphy of the Cenomanian–Turonian Oceanic Anoxic Event OAE2 in shallow shelf sequences of NE Egypt: Cretaceous Research, v. 32, no. 6, p. 705-722.

Forster, A., Kuypers, M. M. M., Turgeon, S. C., Brumsack, H.-J., Petrizzo, M. R., and Sinninghe Damsté, J. S., 2008, The Cenomanian/Turonian Oceanic Anoxic Event in the South Atlantic: New insights from a geochemical study of DSDP Site 530A: Palaeogeography, Palaeoclimatology, Palaeoecology, v. 267, no. 3-4, p. 256-283.

Frey, F., Coffin, M., Wallace, P., Weis, D., Zhao, X., Wise Jr, S., Wähnert, V., Teagle, D., Saccocia, P., and Reusch, D., 2000, Origin and evolution of a submarine large igneous province: the Kerguelen Plateau and Broken Ridge, southern Indian Ocean: Earth and Planetary Science Letters, v. 176, no. 1, p. 73-89.

Friedrich, O., Erbacher, J., Moriya, K., Wilson, P. A., and Kuhnert, H., 2008, Warm saline intermediate waters in the Cretaceous tropical Atlantic Ocean: Nature Geoscience, v. 1, no. 7, p. 453-457.

Gertsch, B., Adatte, T., Keller, G., Tantawy, A. A. A. M., Berner, Z., Mort, H. P., and Fleitmann, D., 2010, Middle and late Cenomanian oceanic anoxic events in shallow and deeper shelf environments of western Morocco: Sedimentology, v. 57, no. 6, p. 1430-1462.

Goldstein, S. J., and Jacobsen, S. B., 1988, Nd and Sr isotopic systematics of river water suspended material: implications for crustal evolution: Earth and Planetary Science Letters, v. 87, no. 3, p. 249-265.

Goldstein, S. L., and Hemming, S. R., 2003, Long-lived isotopic tracers in oceanography, paleoceanography, and ice-sheet dynamics: Treatise on Geochemistry, v. 6, p. 453-489.

Gradstein, F. M., 1992, 43. Legs 122 and 123, Northwestern Australian Margin- A stratigraphic and Paleogeographic Summary: Proceedings of the Ocean Drilling Program, Scientific Results, v. 123, p. 801-816.

Hague, A. M., Thomas, D. J., Huber, M., Korty, R., Woodard, S. C., and Jones, L. B., 2012, Convection of North Pacific deep water during the early Cenozoic: Geology, v. 40, no. 6, p. 527-530.

Halliday, A. N., Davidson, J. P., Holden, P., Owen, R. M., and Olivarez, A. M., 1992, Metalliferous sediments and the scavenging residence time of Nd near hydrothermal vents: Geophysical Research Letters, v. 19, no. 8, p. 761-764.

Haq, B. U., Boyd, R. L., Exon, N. F., and Rad, U. v., 1992, Evolution of the Central Exmouth Plateau: A post-drilling perspective: Proceedings of the Ocean Drilling Program, Scientific Results, v. 122, p. 801-816.

Hasegawa, H., Tada, R., Jiang, X., Suganuma, Y., Imsamut, S., Charusiri, P., Ichinnorov, N., and Khand, Y., 2012, Drastic shrinking of the Hadley circulation during the mid-Cretaceous Supergreenhouse: Climate of the Past, v. 8, no. 4, p. 1323-1337.

Haupt, B. J., and Seidov, D., 2001, Warm deep-water ocean conveyor during Cretaceous time: Geology, v. 29, no. 4, p. 295-298.

Haworth, M., Hesselbo, S. P., McElwain, J. C., Robinson, S. A., and Brunt, J. W., 2005, Mid-Cretaceous pCO2 based on stomata of the extinct conifer Pseudofrenelopsis (Cheirolepidiaceae): Geology, v. 33, no. 9, p. 749-752.

Hay, W. W., 2008, Evolving ideas about the Cretaceous climate and ocean circulation: Cretaceous Research, v. 29, no. 5-6, p. 725-753.

Hay, W. W., DeConto, R. M., Wold, C. N., Wilson, K. M., Voigt, S., Schulz, M., Wold, A. R., Dullo, W.-C., Ronov, A. B., Balukhovsky, A. N., and Soding, E., 1999, Alternative global Cretaceous paleogeography: Evolution of the Cretaceous Ocean-Climate System, p. 1.

Heine, C., Müller, R. D., and Gaina, C., 2004, Reconstructing the lost eastern Tethys Ocean Basin: Convergence history of the SE Asian margin and marine gateways: Geophysical Monograph Series, v. 149, p. 37-54.

Hu, X., Wang, C., Li, X., Fan, S., and Peng, P. a., 2001, The Cenomanian-Turonian Anoxic Event in southern Tibet: A study of organic geochemistry: Chinese Journal of Geochemistry, v. 20, no. 4, p. 289-295.

Huber, B. T., Hodell, D. A., and Hamilton, C. P., 1995, Middle–Late Cretaceous climate of the southern high latitudes: Stable isotopic evidence for minimal equator-to-pole thermal gradients: Geological Society of America Bulletin, v. 107, no. 10, p. 1164-1191.

Huber, B. T., Norris, R. D., and MacLeod, K. G., 2002, Deep-sea paleotemperature record of extreme warmth during the Cretaceous: Geology, v. 30, no. 2, p. 123.

Jarvis, I., Carson, G., Cooper, M., Hart, M., Leary, P., Tocher, B., Horne, D., and Rosenfeld, A., 1988, Microfossil assemblages and the Cenomanian-Turonian (Late Cretaceous) Oceanic Anoxic Event: Cretaceous Research, v. 9, no. 1, p. 3-103.

Jarvis, I., Lignum, J. S., Gröcke, D. R., Jenkyns, H. C., and Pearce, M. A., 2011, Black shale deposition, atmospheric CO2drawdown, and cooling during the Cenomanian-Turonian Oceanic Anoxic Event: Paleoceanography, v. 26, no. 3.

Jenkyns, H., 1985, The Early Toarcian and Cenomanian-Turonian anoxic events in Europe: comparisons and contrasts: Geologische Rundschau, v. 74, no. 3, p. 505-518.

Jenkyns, H. C., 1980, Cretaceous anoxic events: from continents to oceans: Journal of the Geological Society, v. 137, no. 2, p. 171-188.

Jenkyns, H. C., 2010, Geochemistry of oceanic anoxic events: Geochemistry, Geophysics, Geosystems, v. 11, no. 3.

Kominz, M. A., Browning, J. V., Miller, K. G., Sugarman, P. J., Mizintseva, S., and Scotese, C. R., 2008, Late Cretaceous to Miocene sea-level estimates from the New Jersey and Delaware coastal plain coreholes: an error analysis: Basin Research, v. 20, no. 2, p. 211-226.

Kuypers, M. M. M., van Breugel, Y., Schouten, S., Erba, E., and Sinninghe Damsté, J. S., 2004, N2-fixing cyanobacteria supplied nutrient N for Cretaceous oceanic anoxic events: Geology, v. 32, no. 10, p. 853.

Lacan, F., and Jeandel, C., 2005, Neodymium isotopes as a new tool for quantifying exchange fluxes at the continent–ocean interface: Earth and Planetary Science Letters, v. 232, no. 3-4, p. 245-257.

MacLeod, K., Londoño, C. I., Martin, E., Berrocoso, Á. J., and Basak, C., 2011, Changes in North Atlantic circulation at the end of the Cretaceous greenhouse interval: Nature Geoscience, v. 4, no. 11, p. 779-782.

MacLeod, K. G., Martin, E. E., and Blair, S. W., 2008, Nd isotopic excursion across Cretaceous Ocean Anoxic Event 2 (Cenomanian-Turonian) in the tropical North Atlantic: Geology, v. 36, no. 10, p. 811.

Manabe, S., and Bryan, K., 1985, CO2-induced change in a coupled ocean-atmosphere model and its paleoclimatic implications: Journal of Geophysical Research: Oceans (1978–2012), v. 90, no. C6, p. 11689-11707.

Martin, E. E., MacLeod, K. G., Jiménez Berrocoso, A., and Bourbon, E., 2012, Water mass circulation on Demerara Rise during the Late Cretaceous based on Nd isotopes: Earth and Planetary Science Letters, v. 327-328, p. 111-120.

Martin, S., Drucker, R., and Yamashita, K., 1998, The production of ice and dense shelf water in the Okhotsk Sea polynyas: Journal of Geophysical Research, v. 103, no. C12, p. 27771.

Meyers, P. A., and Snowdon, L., 1992, 52. Data Report: Extractable hydrocarbon and carbon isotope geochemistry of Lower Cretaceous sediments from Sites 762 and 763 on the Exouth Plateau, northwest Australian margin: Proceedings of the Ocean Drilling Program, Scientific Results, v. 122.

Meyers, P. A., Yum, J.-G., and Wise, S. W., 2009, Origins and maturity of organic matter in mid-Cretaceous black shales from ODP Site 1138 on the Kerguelen Plateau: Marine and Petroleum Geology, v. 26, no. 6, p. 909-915.

Monteiro, F. M., Pancost, R. D., Ridgwell, A., and Donnadieu, Y., 2012, Nutrients as the dominant control on the spread of anoxia and euxinia across the Cenomanian-Turonian Oceanic Anoxic Event (OAE2): Model-data comparison: Paleoceanography, v. 27, no. 4.

Moriya, K., 2011, Development of the Cretaceous Greenhouse Climate and the Oceanic Thermal Structure: Paleontological Research, v. 15, no. 2, p. 77-88.

Murphy, D. P., and Thomas, D. J., 2012, Cretaceous deep-water formation in the Indian sector of the Southern Ocean: Paleoceanography, v. 27, no. 1.

Otto-Bliesner, B. L., Brady, E. C., and Shields, C., 2002, Late Cretaceous ocean: Coupled simulations with the National Center for Atmospheric Research climate system model: Journal of Geophysical Research: Atmospheres (1984–2012), v. 107, no. D2, p. ACL 11-11-ACL 11-14.

Palmer, M., and Elderfield, H., 1986, Rare earth elements and neodymium isotopes in ferromanganese oxide coatings of Cenozoic foraminifera from the Atlantic Ocean: Geochimica et Cosmochimica Acta, v. 50, no. 3, p. 409-417.

Pearce, M. A., Jarvis, I., and Tocher, B. A., 2009, The Cenomanian–Turonian boundary event, OAE2 and palaeoenvironmental change in epicontinental seas: New insights from the dinocyst and geochemical records: Palaeogeography, Palaeoclimatology, Palaeoecology, v. 280, no. 1-2, p. 207-234.

Pedersen, T., and Calvert, S., 1990, Anoxia vs. Productivity: What Controls the Formation of Organic-Carbon-Rich Sediments and Sedimentary Rocks?(1): AAPG Bulletin, v. 74, no. 4, p. 454-466.

Piepgras, D. J., Wasserburg, G., and Dasch, E., 1979, The isotopic composition of Nd in different ocean masses: Earth and Planetary Science Letters, v. 45, no. 2, p. 223-236.

Poulsen, C. J., Barron, E. J., Arthur, M. A., and Peterson, W. H., 2001, Response of the Mid-Cretaceous global oceanic circulation to tectonic and CO2forcings: Paleoceanography, v. 16, no. 6, p. 576-592.

Pucéat, E., 2008, A new breath of life for anoxia: Geology, v. 36, no. 10, p. 831-832.

Retallack, G. J., 2001, A 300-million-year record of atmospheric carbon dioxide from fossil plant cuticles: Nature, v. 411, no. 6835, p. 287-290.

Robinson, S. A., and Vance, D., 2012, Widespread and synchronous change in deep-ocean circulation in the North and South Atlantic during the Late Cretaceous: Paleoceanography, v. 27, no. 1.

Sarmiento, J. L., Herbert, T. D., and Toggweiler, J., 1988, Causes of anoxia in the world ocean: Global Biogeochemical Cycles, v. 2, no. 2, p. 115-128.

Schlanger, S., and Jenkyns, H., 1976, Cretaceous oceanic anoxic events: causes and consequences: Geologie en mijnbouw, v. 55, no. 3-4, p. 179-184.

Tachikawa, K., Jeandel, C., and Roy-Barman, M., 1999, A new approach to the Nd residence time in the ocean: the role of atmospheric inputs: Earth and Planetary Science Letters, v. 170, no. 4, p. 433-446.

Talley, L. D., 1993, Distribution and formation of North Pacific intermediate water: Journal of Physical Oceanography, v. 23, no. 3, p. 517-537.

Thomas, D. J., 2004, Evidence for deep-water production in the North Pacific Ocean during the early Cenozoic warm interval: Nature, v. 430, no. 6995, p. 65-68.

Tissot, B., Demaison, G., Masson, P., Delteil, J., and Combaz, A., 1980, Paleoenvironment and petroleum potential of middle Cretaceous black shales in Atlantic basins: AAPG Bulletin, v. 64, no. 12, p. 2051-2063.

Totman Parrish, J., and Curtis, R. L., 1982, Atmospheric circulation, upwelling, and organic-rich rocks in the Mesozoic and Cenozoic eras: Palaeogeography, Palaeoclimatology, Palaeoecology, v. 40, no. 1, p. 31-66.

Trabucho Alexandre, J., Tuenter, E., Henstra, G. A., van der Zwan, K. J., van de Wal, R. S. W., Dijkstra, H. A., and de Boer, P. L., 2010, The mid-Cretaceous North Atlantic nutrient trap: Black shales and OAEs: Paleoceanography, v. 25, no. 4.

Tyson, R., 2005, The" productivity versus preservation" controversy: cause, flaws, and resolution: Special Publication-SEPM, v. 82, p. 17.

Tyson, R. V., 1996, Sequence-stratigraphical interpretation of organic facies variations in marine siliciclastic systems: general principles and application to the onshore Kimmeridge Clay Formation, UK: Geological Society, London, Special Publications, v. 103, no. 1, p. 75-96.

Tyson, R. V., and Pearson, T. H., 1991, Modern and ancient continental shelf anoxia: an overview: Geological Society, London, Special Publications, v. 58, no. 1, p. 1-24.

Voigt, S., Gale, A. S., and Flögel, S., 2004, Midlatitude shelf seas in the Cenomanian-Turonian greenhouse world: Temperature evolution and North Atlantic circulation: Paleoceanography, v. 19, no. 4.

von Blanckenburg, F., 1999, Tracing past ocean circulation?: Science, v. 286, no. 5446, p. 1862-1863.

Westermann, S., Caron, M., Fiet, N., Fleitmann, D., Matera, V., Adatte, T., and Föllmi, K. B., 2010, Evidence for oxic conditions during Oceanic Anoxic Event 2 in the northern Tethyan pelagic realm: Cretaceous Research, v. 31, no. 5, p. 500-514.

Wilson, P. A., and Norris, R. D., 2001, Warm tropical ocean surface and global anoxia during the mid-Cretaceous period: Nature, v. 412, no. 6845, p. 425-429.

Wilson, P. A., Norris, R. D., and Cooper, M. J., 2002, Testing the Cretaceous greenhouse hypothesis using glassy foraminiferal calcite from the core of the Turonian tropics on Demerara Rise: Geology, v. 30, no. 7, p. 607-610.

Yasuda, I., 1997, The origin of the North Pacific Intermediate Water: Journal of Geophysical Research, v. 102, no. C1, p. 893.

Zhang, Y., Lacan, F., and Jeandel, C., 2008, Dissolved rare earth elements tracing lithogenic inputs over the Kerguelen Plateau (Southern Ocean): Deep Sea Research Part II: Topical Studies in Oceanography, v. 55, no. 5-7, p. 638-652.

APPENDIX

Site	Sample ID	Depth (mbsf)	Age (Ma)	143Nd/144Nd	Absolute Error (2σ)	$\varepsilon_{Nd}(t)$	Error (2σ)
				Hole 763B, Indian Ocean			
763B	19X-3, 61-62	355.10	88.55	0.512197	0.0000026	-7.9	0.05
763B	19X-6, 61-63	359.62	89.23	0.512181	0.0000021	-8.2	0.04
763B	20X-1, 33.5-34.5	361.34	89.49	0.512204	0.0000020	-7.7	0.04
763B	20X-2, 95-96	363.46	89.81	0.512204	0.0000031	-7.7	0.06
763B	21X-1, 8-9	370.59	90.89	0.512109	0.0000024	-9.6	0.05
763B	21X-1, 118.5-119.5	371.69	91.06	0.512145	0.0000018	-8.9	0.03
763B	21X-2, 69-70	372.70	91.21	0.512100	0.0000025	-9.7	0.05
763B	22X-1, 85.5-86.5	380.86	92.45	0.512032	0.0000203	-11.0	0.40
763B	22X-2, 18-19	381.69	92.58	0.512039	0.0000023	-10.9	0.04
763B	23X-1, 43-44	389.94	93.69	0.512052	0.0000019	-10.7	0.04
763B	23X-2, 33-34	391.34	93.88	0.512055	0.0000021	-10.6	0.04
763B	23X-4, 55-56	394.56	94.37	0.512032	0.0000034	-11.0	0.07
763B	23X-5, 41.5-42.5	395.92	94.55	0.512053	0.0000024	-10.6	0.05
763B	24X-7, 30.5-31.5	408.31	96.23	0.512056	0.0000026	-10.5	0.05
763B	25X-1, 45-46	408.96	96.32	0.512070	0.0000011	-10.3	0.02
763B	25X-3, 50.5-51.5	412.01	96.73	0.512067	0.0000024	-10.3	0.05
763B	26-3, 81-82	421.81	98.05	0.512090	0.0000035	-9.9	0.07
763B	27-4, 85-86	432.85	99.54	0.512109	0.0000030	-9.5	0.06
763B	28-4, 82-84	442.35	100.83	0.512086	0.0000044	-9.9	0.08

Hole 765C, Indian Ocean

765C	25R-3, 61-62	582.60	89.67	0.512249	0.0000007	-6.8	0.01
765C	25R-5,49.5-50.5	585.53	91.62	0.512220	0.0000034	-7.4	0.07
765C	26R-1, 4-5	588.34	93.49	0.512226	0.0000055	-7.3	0.11
765C	26R-1, 34-35	588.64	93.69	0.512242	0.0000038	-6.9	0.07
765C	26R-1, 57-58	588.87	93.85	0.512262	0.0000063	-6.5	0.12
765C	26R-1, 84-85	589.13	94.04	0.512210	0.0000021	-7.6	0.04
765C	26R-1, 136-137	589.65	94.79	0.512249	0.0000100	-6.8	0.20
765C	26R-2, 7.5-8.5	589.83	95.04	0.512244	0.0000035	-6.9	0.07
765C	26R-2, 24-25	589.98	95.26	0.512190	0.0000024	-7.9	0.05
765C	26R-2, 55.5-56.5	590.30	95.71	0.512193	0.0000026	-7.9	0.05
765C	26R-2, 64-65	590.40	95.86	0.512193	0.0000026	-7.9	0.05
765C	26R-4, 28-29	592.93	99.47	0.512152	0.0000028	-8.6	0.05

Hole 766A, Indian Ocean

766A	14R-4, 146.5-147.5	129.56	90.72	0.512214	0.0000016	-7.5	0.03
766A	14R-5, 70.5-71.5	130.30	91.03	0.512242	0.0000018	-7.0	0.04
766A	15R-1, 8-9	133.26	92.26	0.512314	0.0000040	-5.5	0.08
766A	15R-1, 115-116	134.35	92.70	0.512251	0.0000073	-6.8	0.14
766A	15R-2, 55-56	135.26	93.76	0.512258	0.0000103	-6.4	0.20
766A	15R-2, 94-95	135.64	94.22	0.512181	0.0000170	-7.9	0.33
766A	15R-3, 12-13	136.32	95.01	0.512152	0.0000028	-8.4	0.06
766A	15R-3 29-30	136.49	95.22	0.512251	0.0000020	-6.5	0.04
766A	15R-3, 38.5-39.5	136.58	95.32	0.512202	0.0000034	-7.4	0.07
766A	15R-3, 46.5-47.5	136.68	95.44	0.512195	0.0000032	-7.6	0.06
766A	15R-3, 99-100	137.20	96.05	0.512172	0.0000035	-8.0	0.07
766A	15R-4, 69-70	138.38	97.44	0.512161	0.0000153	-8.2	0.30
766A	15R-5, 100-101	140.20	98.99	0.512149	0.0000024	-8.7	0.05

Hole 1138A, Indian Ocean

1138A	67-2, 5-6	632.17	85.94	0.512248	0.0000029	-6.9	0.06
1138A	67-2, 75-76	632.87	86.06	0.512313	0.0000026	-5.6	0.05
1138A	68-1, 6-7	640.47	87.35	0.512239	0.0000023	-7.0	0.05
1138A	68-1, 42.5-43.5	640.83	87.41	0.512247	0.0000031	-6.9	0.06
1138A	68-2, 36-37	643.62	93.13	0.512218	0.0000021	-7.4	0.04
1138A	68-3, 21-22	644.88	93.31	0.512495	0.0000057	-2.0	0.11
1138A	68-4, 25.5-26.5	645.82	93.45	0.512206	0.0000029	-7.7	0.06
1138A	69-2, 52.5-53.5	651.95	93.50	0.512176	0.0000022	-8.2	0.04
1138A	69-3, 23.5-24.5	652.83	93.51	0.512203	0.0000036	-7.7	0.07
1138A	69-5, 60-61	656.18	93.56	0.512156	0.0000026	-8.6	0.05
1138A	69-6, 52-53	657.60	93.58	0.512326	0.0000081	-5.3	0.16
1138A	70-1, 17.5-18.5	659.78	93.61	0.512453	0.0000055	-2.8	0.11
1138A	70-1, 130-131	660.95	93.63	0.512452	0.0000047	-2.8	0.09
1138A	70-2, 56-57	661.67	93.64	0.512472	0.0000037	-2.5	0.07
1138A	71-2, 60-62	671.10	93.78	0.512522	0.0000028	-1.5	0.05
1138A	72-2, 20-21	680.60	93.92	0.512633	0.0000041	0.7	0.08
1138A	73-2, 46-47	689.75	94.05	0.512616	0.0000049	0.4	0.10